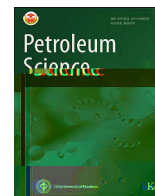




Contents lists available at ScienceDirect

Petroleum Science

journal homepage: www.keaipublishing.com/en/journals/petroleum-science

Original Paper

Advancing CCUS-EOR in low-permeability reservoirs with surfactant-enhanced carbonated water and CO₂ alternating flooding: An integrated experimental and numerical investigation

Xiao-Bing Han^a, Hai-Yang Yu^{a,*}, Tong-Bing Wang^a, Peng Song^b, Jia-Bang Song^a, Lu Liu^a, Hui-Ting Tang^a, Jun Lu^c, Yang Wang^{a,**}^a State Key Laboratory of Petroleum Resources and Engineering, China University of Petroleum (Beijing), Beijing, 102249, China^b Research Institute of Exploration and Development, PetroChina Changqing Oilfield Company, Xi'an, Shaanxi, 710018, China^c McDougall School of Petroleum Engineering, The University of Tulsa, Tulsa, OK, 74104, USA

ARTICLE INFO

Article history:

Received 20 May 2025

Received in revised form

25 July 2025

Accepted 30 November 2025

Available online 3 December 2025

Edited by Teng Zhu and Min Li

Keywords:

Enhanced water alternating gas

Sweep efficiency

Oil displacement efficiency

CO₂ storage efficiency

ABSTRACT

Surfactant-enhanced carbonated water alternating with CO₂ (SCWAG) flooding, which integrates the advantages of surfactants, carbonated water (CW), and CO₂, has demonstrated significant potential for the development of low-permeability reservoirs. Nonetheless, the underlying mechanisms of SCWAG-enhanced oil recovery require further elucidation. Its CO₂ storage performance and pore-scale oil displacement characteristics have not been thoroughly investigated, and the influence of various factors on SCWAG performance remains poorly understood. This study, for the first time, investigates the pore-scale oil displacement characteristics and CO₂ storage performance of SCWAG by integrating core flooding experiments and nuclear magnetic resonance scanning. An innovative core-scale 3D heterogeneous numerical model was developed using computed tomography scanning and refined via history matching, thereby enabling reliable SCWAG simulation and facilitating reservoir-scale analysis of factors affecting SCWAG performance. The results demonstrate that SCWAG notably improves both sweep efficiency and oil displacement efficiency, achieving higher recovery and CO₂ storage efficiency than other methods. The total recovery reached 76.99%, with individual recoveries of 56.35%, 76.85%, and 87.96% for micropores, mesopores, and macropores, respectively, while the CO₂ storage efficiency is 57.22%. Permeability contrast exerts a significant effect on recovery, whereas CO₂ storage efficiency was primarily influenced by the injection rate and water-to-gas ratio. Moreover, the interaction between the water-to-gas ratio and permeability contrast exerts a substantial impact on both recovery and CO₂ storage efficiency. This study provides novel insights and an in-depth analysis of the SCWAG process, offering practical guidelines for its application in low-permeability reservoirs.

© 2025 The Authors. Publishing services by Elsevier B.V. on behalf of KeAi Communications Co. Ltd. This is an open access article under the CC BY-NC-ND license (<http://creativecommons.org/licenses/by-nc-nd/4.0/>).

1. Introduction

The large-scale emission of greenhouse gases (e.g., CO₂, methane, water vapor) from human activities has intensified the greenhouse effect, accelerating global warming. As the most

concerning anthropogenic greenhouse gas, CO₂ is a critical driver of this phenomenon and thus one of the primary targets for mitigation strategies (Cui et al., 2024; Filonchik et al., 2024; Zhou et al., 2025). In response, Carbon Capture, Utilization, and Storage (CCUS) technologies have been proposed, among which CO₂ flooding enhanced oil recovery (EOR) represents a pivotal approach. This method not only enhances oil recovery but also facilitates CO₂ sequestration (Gao et al., 2025; Lin et al., 2022; Liu and Rui, 2022). The high solubility of CO₂ in oil reduces oil viscosity, induces volume expansion, and lowers interfacial tension (IFT), resulting in superior displacement efficiency (Bai et al., 2025; Liu et al., 2025; Song et al., 2025). Nevertheless, the significant

* Corresponding author.

** Corresponding author.

E-mail addresses: haiyangyu.cup@139.com (H.-Y. Yu), petroyang@cup.edu.cn (Y. Wang).

Peer review under the responsibility of China University of Petroleum (Beijing).

differences in viscosity and density between CO₂ and oil result in an unstable displacement front, increasing the risk of gas breakthrough and ultimately reducing sweep efficiency (Luo et al., 2023).

Sweep efficiency is a critical factor that limits the effectiveness of CO₂ development. Water-alternating-gas (WAG) flooding is an effective method for controlling gas breakthrough and improving sweep efficiency (Afzali et al., 2018). The primary mechanism of this method is the alternating flooding of water and gas slugs, which achieves mobility control, stabilizes the displacement front, increases the flow resistance of CO₂, and compels it to enter low-permeability areas, thereby expanding sweep efficiency (Hao et al., 2016). He et al. (2023) simulated WAG injection in a micromodel, analyzing time-varying fingerings and pattern crossovers under three-phase flow conditions. They observed that pressure difference significantly influenced fingering pattern changes. Furthermore, even a small amount of water notably affected the fingering patterns during WAG flooding. Through micro-numerical simulations, they also discovered that CO₂ dissolution into crude oil could suppress fingering phenomena, and that the resulting reduction in crude oil viscosity could inhibit viscous fingering (He et al., 2024). Wang et al. (2020) conducted microfluidic experiments, and the results demonstrated that compared to CO₂ flooding, WAG improved volumetric sweep efficiency by 32.5%, while oil recovery rose by 23.15%. Meanwhile, core displacement experiments using nuclear magnetic resonance (NMR) by Xiao et al. (2017) revealed that WAG significantly improved EOR performance in small pores, achieving a 4.09% increase compared to CO₂ flooding. Field applications have demonstrated that WAG can increase recovery by 5%–10%, while also effectively storing CO₂. Vo Thanh et al. (2020) performed numerical simulations of the Nam Vang oilfield and demonstrated that, in comparison with CO₂ flooding, WAG improved CO₂ storage efficiency by approximately 25%. Although WAG has yielded positive results, it is prone to water shielding, in which the injected water acts as a barrier, preventing direct contact between the injected CO₂ and oil, thereby reducing displacement efficiency (Dong et al., 2005; Majidaie et al., 2012; Tiffin and Yellig, 1983). Furthermore, while w

performance, a core-scale 3D heterogeneous numerical model, constrained by computed tomography (CT) scanning data and history matching, was developed, thereby enabling reliable SCWAG simulation and facilitating reservoir-scale numerical simulations coupled with response surface methodology (RSM). These findings offer novel insights into the research and application of SCWAG, contributing to both EOR and the achievement of CO₂ storage.

2. Core flooding experiments

2.1. Materials

2.1.1. Cores

Core samples were sourced from Daqing Oilfield in China, with a burial depth of approximately 2200 m. After cutting and cleaning, the core length was about 10.0 cm, and the diameter was approximately 2.5 cm. Core porosity and permeability were measured using the QKY-1 porosity measuring device and the PDP-200 permeability device, respectively. Cores with comparable porosity and permeability were selected for experiments, with an average porosity of 15.80% and an average permeability of 14.54 mD. The cores were primarily composed of quartz. Specific petrophysical parameters of the cores are detailed in Table 1.

2.1.2. Oil

Under reservoir conditions of temperature (72 °C) and pressure (25 MPa), the density of the formation oil is 0.709 g/cm³, and its viscosity is 0.494 mPa·s. Its saturation pressure is 9.532 MPa, with a gas-to-oil ratio of 96.61 m³/m³. Stock tank oil from the target reservoir and its associated gas were utilized to prepare live oil, with a gas-to-oil ratio adjusted to match that of the formation oil, for use in the experiments. The specific composition of the oil, as shown in Fig. 1, reveals that light components predominate, with the C₁–C₁₅ fractions accounting for 82.76 mol%. The results of slim-tube experiments demonstrate that the minimum miscibility pressure between CO₂ and crude oil is approximately 20.0 MPa under reservoir temperature. Therefore, miscible CO₂ flooding is considered feasible in the target reservoir.

2.1.3. Surfactant

The surfactant used in the experiment was sourced from the oilfield. It is a zwitterionic surfactant capable of withstanding high temperatures and high salinity, significantly improving wettability and reducing IFT. The critical micelle concentration of the surfactant is 0.03 w.t.%, and considering the potential loss of surfactant during the displacement process, a concentration of 0.10 w.t.% was employed in the experiment, which is the same as that used in the oilfield. To shield the hydrogen signal in water and enable the measurement of recovery in pores of different sizes using NMR, 12.0 w.t.% manganese chloride was added to the surfactant solution, which was subsequently used to prepare the surfactant solution. Under the target reservoir temperature conditions, the IFT between the surfactant solution and oil was 0.08

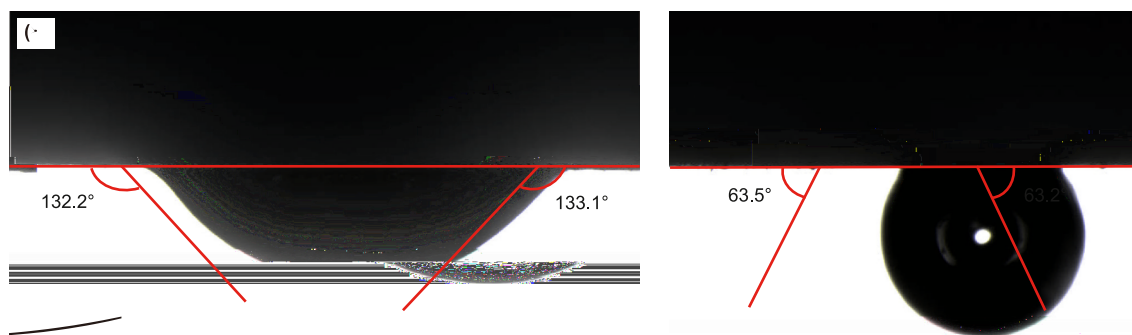


Fig. 2. Comparison of contact angle. (a) Before contact with surfactant; (b) After contact with surfactant.

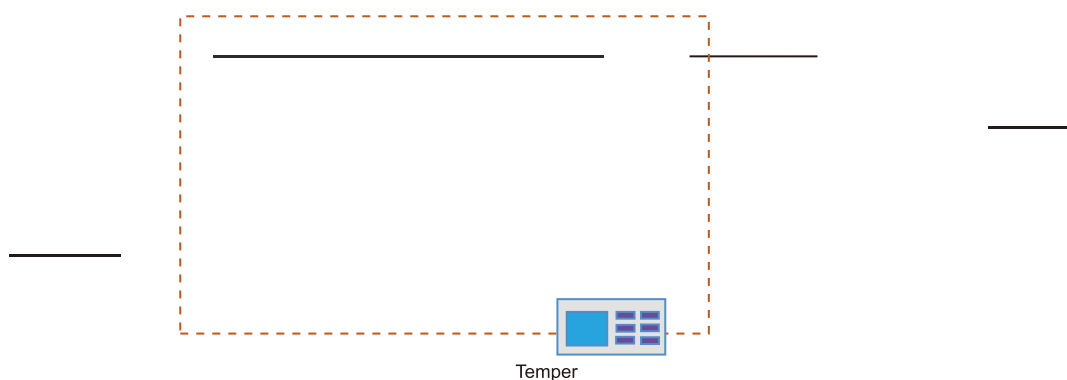


Fig. 3. Schematic diagram of the displacement experimental device.

pores of varying sizes. The specific experimental steps are outlined below:

- (1) The core is evacuated for 24 h and then saturated with distilled water for 48 h prior to NMR scanning.
- (2) The experimental apparatus is assembled, and a 12 w.t.% manganese chloride solution is injected at a constant flow rate of 0.1 mL/min to suppress the hydrogen signal. After injecting a total of 20 pore volumes, NMR scanning is conducted.
- (3) The temperature is adjusted to 72 °C, the pressure to 25 MPa, and the confining pressure is maintained at 3 MPa above the injection pressure. Oil is injected into the core until no water is observed at the outlet, establishing bound water saturation. Subsequently, the core is aged for 72 h and subjected to NMR scanning again.
- (4) CO₂ is used to displace the core at a rate of 0.1 mL/min. The injection is terminated after a cumulative volume of 1.2 pore volume (PV) has been injected. Subsequently, an NMR scan is conducted to quantify the oil recovery. During the displacement, oil production is measured at various CO₂ injection volumes to obtain the oil recovery curve. Simultaneously, the produced gas is collected and quantified, and its composition is analyzed via gas chromatography to calculate CO₂ storage efficiency.
- (5) The experimental core is replaced; steps (1) to (3) are repeated to re-establish initial conditions, after which WAG, CWAG, and SCWAG flooding is performed as in step (4). For both CWAG and SCWAG flooding experiments, the change in contact angle before and after the experiment is measured using the sessile drop method.

Notably, for both WAG and SCWAG flooding, the slug size is 0.1 PV. Additionally, for the SCWAG experimental core, CT scanning is conducted after evacuation, followed by CT scanning after saturation with experimental water, before displacement experiments are performed. Additionally, certain experimental uncertainties are present. For oil recovery measurements and contact angle determination, the dominant source of error is human-induced, primarily due to reading inaccuracies. For CO₂ storage efficiency, the errors are predominantly systematic, originating from the gas flow meter measurement and chromatographic analysis. Therefore, to account for the influence of these uncertainties, appropriate error bars were added to the experimental data, providing a more comprehensive and accurate representation of the results.

2.3. Quantitative analysis method of NMR

NMR scanning can be employed to obtain the transverse relaxation time distribution spectrum, commonly known as the T₂

spectrum, by detecting NMR signals from hydrogen-containing fluids within porous media. The transverse relaxation time of fluids in porous media is influenced by the combined effects of bulk relaxation, surface relaxation, and diffusion relaxation, which can be expressed as Eq. (1) (Tang et al.,

SCWAG enables SCW to penetrate smaller core pores and contact oil, thereby facilitating CO₂ mass transfer and improving microscopic sweep efficiency and oil displacement efficiency. Furthermore, the acidic environment generated by SCW could protonate the zwitterionic surfactant, potentially leading to enhanced adsorption at the oil-water interface and on the rock surface, further improving wettability and reducing IFT (Sarkar et al., 2021).

2.4.2. CO₂ storage efficiency

Fig. 9 provides a comparison of CO₂ storage efficiency across

(Nowrouzi et al., 2019). As shown in Fig. 8, following CWAG flooding, the contact angle decreased from 129.6° to 97.1°. In contrast, SCWAG flooding significantly improved wettability, reducing the contact angle from 135.2° to 49.5°. Consequently,

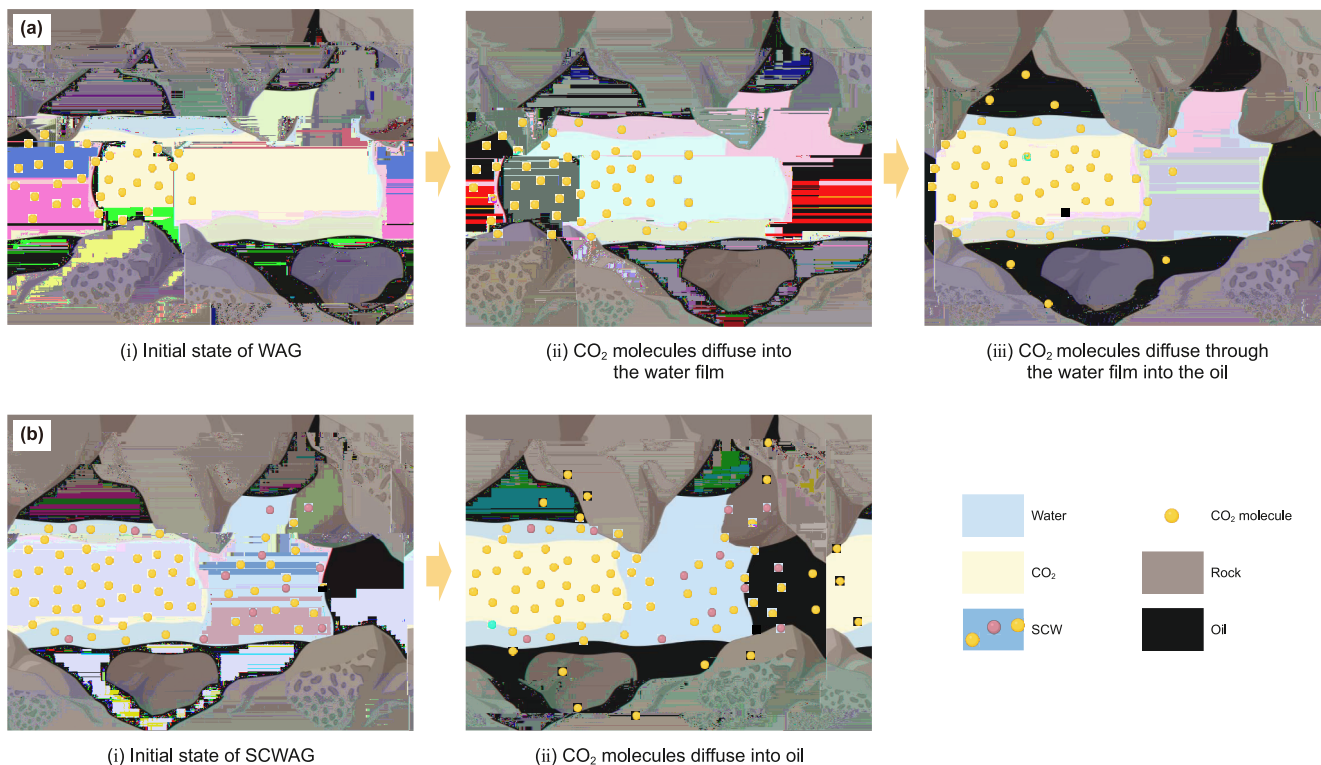


Fig. 7. Schematic illustration of the mechanism by which SCWAG mitigates the water shielding. **(a)** Process of CO₂ transfer to oil during WAG flooding; **(b)** Process of CO₂ transfer to oil during SCWAG flooding.

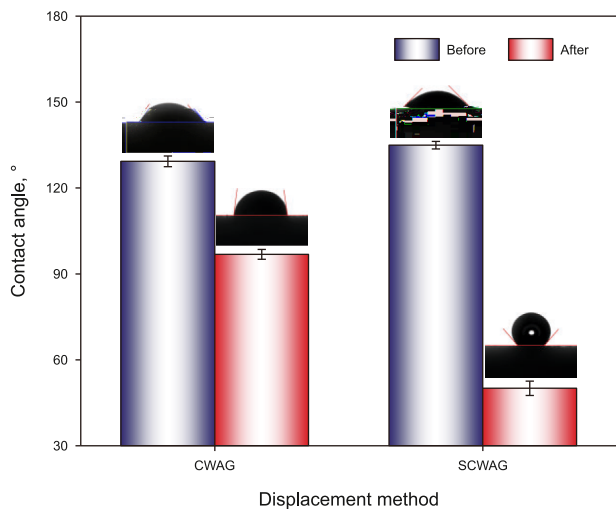


Fig. 8. Comparison of contact angle changes before and after SCWAG and CWAG flooding.

In contrast, WAG flooding stabilized the gas displacement front through alternating injections of water and gas, effectively suppressing gas breakthrough. This enabled more oil to be displaced from core pores, thereby providing increased pore space for CO₂ storage. Furthermore, CO₂ dissolved not only in bound water and residual oil but also in injected water, further enhancing dissolved CO₂ storage in water. Consequently, the CO₂ storage efficiency for WAG flooding significantly increased to 55.60%.

Although CWAG mitigated the effects of water shielding and achieved higher recovery, CO₂ was pre-dissolved in CW, necessitating a larger CO₂ injection volume. Moreover, CW had limited capacity to further dissolve injected CO₂, resulting in a slightly

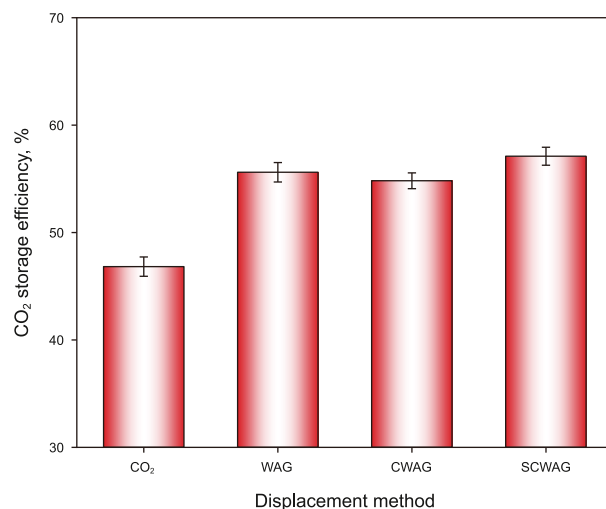


Fig. 9. CO₂ storage efficiency comparison for different displacement methods.

lower CO₂ storage efficiency compared with WAG. SCWAG further enhanced recovery, expanded the pore space available for CO₂ storage, and enhanced CO₂ mass transfer. As a result, CO₂ storage efficiency rose to 57.22%, surpassing both WAG and CWAG.

3. Numerical simulation

3.1. Modeling of carbonated water

The setup for the CW simulation in the numerical simulation software followed the methodology described by Ji et al. (2023).

The key to numerical simulation of CW lies in describing the solubility differences of CO₂ in oil and water, which are determined by the partition coefficient of CO₂ between oil and water (Yang et al., 2019). The CO₂ partition coefficient is defined as the ratio of its effective molar fractions in the oil and water phases, as expressed in Eq. (6) (Li and Nghiem, 1986):

$$\log p = \log \frac{c_o}{c_w} \quad (6)$$

where, c_o and c_w are the CO₂ molar fractions in the oil and water phases, respectively.

The molar fraction of CO₂ in the liquid phase can be expressed using fugacity and Henry's constant, as shown in Eq. (7) (Nghiem et al., 1983):

$$f_{iw} = x_i H_i \quad (7)$$

where, f_{iw} is fugacity of component i in the liquid phase, Pa; x_i is molar fraction of component i ; H_i is Henry's constant of component i , Pa.

The Henry's constant is a function of temperature and pressure, which can be calculated using Eq. (8):

$$\ln H_i = \ln H_i^* + \frac{i(p - p^*)}{RT} \quad (8)$$

where, p^* is reference pressure, Pa; H_i^* is value of Henry's constant at p^* , Pa; T is temperature, K; R is ideal gas constant, J/(mol⁻¹·K⁻¹).

Under the isothermal condition, H_i^* for CO₂ can be calculated using Eq. (9) (Harvey, 1996):

$$\begin{aligned} \ln(H_i^*) = & \ln(p_{H_2O}^*) - A(T_{r,H_2O})^{-1} + B(1 - T_{r,H_2O})^{0.355} (T_{r,H_2O})^{-1} \\ & + C \exp(1 - T_{r,H_2O}) (T_{r,H_2O})^{-0.41} \end{aligned} \quad (9)$$

where, $p_{H_2O}^*$ is saturated vapor pressure of water, MPa; T_{r,H_2O} is reduced temperature of water, K. A, B, and C are constants, A = -9.4234, B = 4.0087, C = 10.3199.

3.2. Establishment of numerical simulation model

3.2.1. Compositional numerical model

Numerical simulations were performed using the compositional model in CMG. The constituent compounds of oil were lumped into pseudo-components to enhance computational efficiency. The parameters of the resulting pseudo-component model were tuned to match the experimental data from constant composition expansion, multi-stage differential liberation, gas expansion, and minimum miscibility pressure experiments. These experimental data adequately captured the intrinsic properties of the crude oil and the interactions between CO₂ and the oil. The fitting results are shown in Fig. 10(a)–(e), demonstrating excellent agreement between the experimental and simulation data. It is noteworthy that the fitting of the minimum miscibility pressure was achieved by integrating PVT fitting with numerical slim tube simulations. Furthermore, the phase diagrams of the pseudo-components and full components were compared (Fig. 10(f)). At the reservoir temperature, the corresponding saturation pressures were 9.529 and 9.509 MPa for the complete composition and pseudo-component model, respectively. These values closely approximated the actual saturation pressure of 9.532 MPa in the target block, with the pseudo-component model exhibiting a saturation pressure error of 0.24%. This comprehensive validation confirmed that the pseudo-component lumping scheme was both

accurate and reliable for subsequent numerical simulations. The specific compositions and characteristic parameters of the pseudo-components are presented in Table 2.

3.2.2. History matching

SCW refers to CW supplemented with surfactants. Therefore, in addition to simulating the transport process of CO₂, it is essential to adjust the relative permeability curves to accurately reflect the effects of both components, thereby enabling the simulation of SCW (Kumar et al., 2021; Lee et al., 2017, 2020). Consequently, a numerical simulation at the experimental scale was established, and the results of laboratory experiments were fitted to refine the relative permeability curves for subsequent reservoir-scale numerical simulation studies. To account for the impact of core heterogeneity on SCWAG flooding and to derive more precise relative permeability curves through history matching, a 3D heterogeneous numerical simulation model reflecting the actual physical properties of the core was constructed using CT scanning. The formula for calculating porosity is presented as Eq. (10) (Akin and Kovscek, 2003):

$$= \frac{CT_{oil} - CT_{air}}{CT_o - CT_a} \quad (10)$$

where CT_{oil} , CT_{air} , CT , and CT_a represent the CT values of oil-saturated cores, air-saturated cores, oil, and air, respectively.

The porosity of the C-4 core is 0.157, and the corresponding permeability is calculated based on the Kozeny-Carman equation as Eq. (11) (Lyu et al., 2021):

$$k = \frac{3D_p^2}{(1 - \phi)^2} \quad (11)$$

where, k is core permeability, mD; ϕ is the proportionality and unity factor, mD/mm²; D_p is average grain size of rock particles, mm; ϕ is core porosity.

The CT scan results are shown in Fig. 11(a), from which the actual porosity distribution was obtained. To enhance the computational efficiency of the model, it was appropriately coarsened, namely resampled. The resampled results are shown in Fig. 11(b). The porosity distribution after resampling closely aligned with the actual core porosity distribution, thereby ensuring the validity and accuracy of the simulation. The resampled data were then utilized to construct a 3D heterogeneous numerical simulation model. The grid sizes in the x , y , and z directions are 13.023, 6.258, and 6.258×10^{-2} cm, respectively, with a total of 98,483 grid blocks.

Based on this numerical simulation model, the injection rate, experimental temperature and pressure were set to align with laboratory experiments. The relative permeability curves were refined, and the CMOST module was utilized to fit the experimental data through history matching. The endpoints of the relative permeability curves, determined from experimental measurements, were 1pr i p T ypoYbeyYOfpT i Ywfl

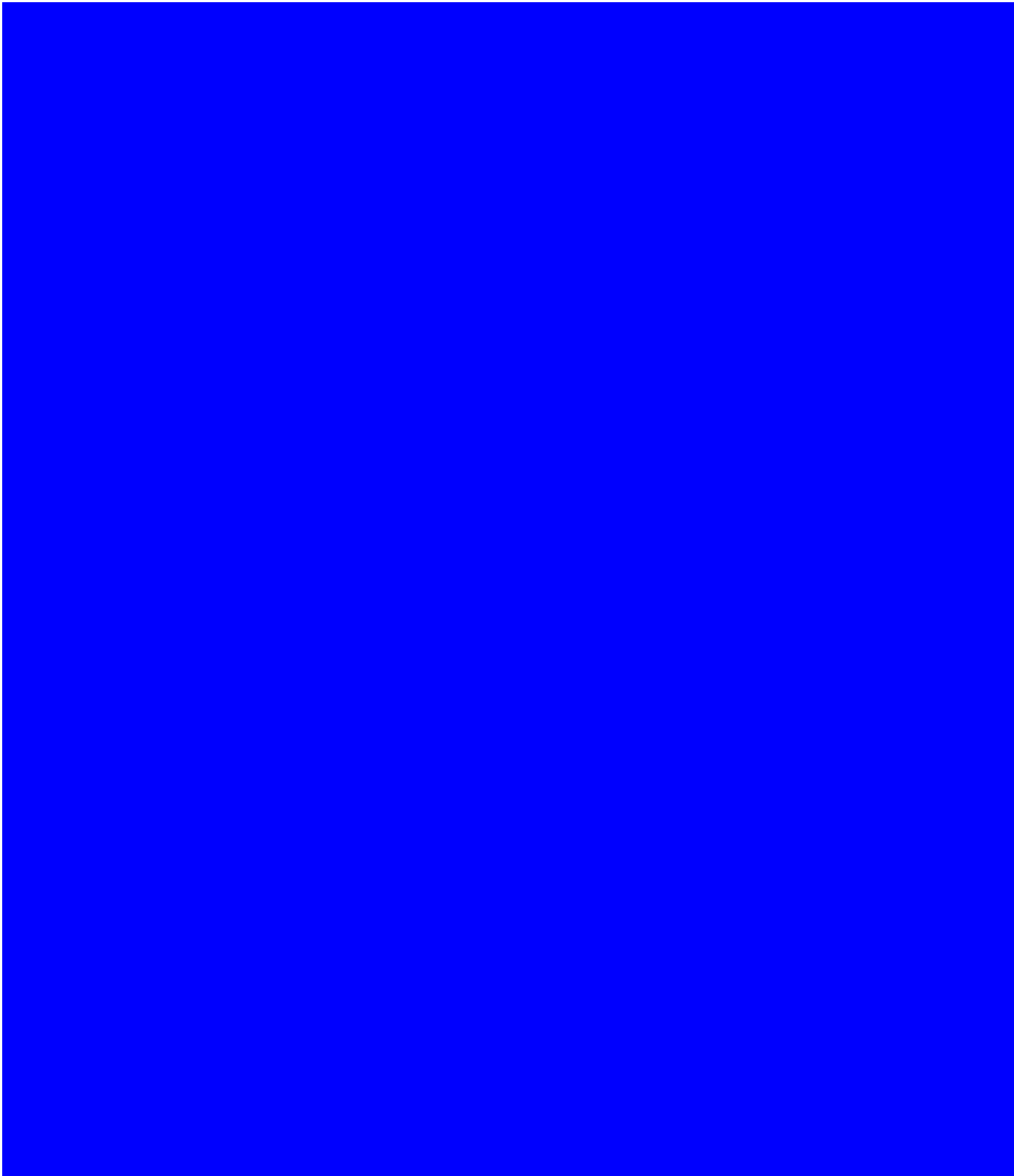


Fig. 10. Fitting results for oil properties and its interaction with CO₂. **(a)** Relative volume; **(b)** Density and viscosity; **(c)** Multistage degassing gas-oil ratio; **(d)** Swelling factor and saturation pressure; **(e)** Minimum miscibility pressure; **(f)** Pressure-temperature phase diagrams.

reservoir-scale numerical simulation model was developed and numerical simulations were conducted, with the ultimate aim of providing a reference for the application of SCWAG in low-permeability reservoirs. The specific parameters of the model, including porosity, permeability, pressure, and temperature, are

detailed in [Table 3](#). To reflect the impact of heterogeneity, the model incorporates a permeability contrast of 5, designating the upper layer as a low-permeability zone and the lower layer as a high-permeability zone. The simulation employed a quarter five-spot pattern, consisting of one injection well and one production

Table 2
Composition and properties of pseudo-components.

Component	Mole fraction, %	Molecular weight, g·mol ⁻¹	V _c , mol ⁻¹	P _c , atm	T _c , K	Acentric factors	Z _c
N ₂	0.918	28.013	0.0895	33.5	126.2	0.04	0.291
CO ₂	0.071	44.010	0.094	72.8	304.2	0.225	0.274
CH ₄	26.045	16.043	0.099	45.4	190.6	0.008	0.288
C ₂ H ₆	6.579	30.070	0.148	48.2	305.4	0.098	0.279
C ₃ H ₈	9.386	44.097	0.203	41.9	369.8	0.152	0.276
C ₄ to C ₇	20.598	72.481	0.302	34.393	471.614	0.241	0.272
C ₈ to C ₁₄	17.792	156.940	0.561	23.639	639.809	0.472	0.269
C ₁₅ to C ₂₁	13.784	288.409	0.916	15.887	758.988	0.747	0.27
C ₂₂ to C ₂₉	4.646	336.715	1.187	12.307	824.753	0.942	0.242
C ₃₀ to C ₃₂	0.182	399.601	1.423	9.982	876.687	1.094	0.229

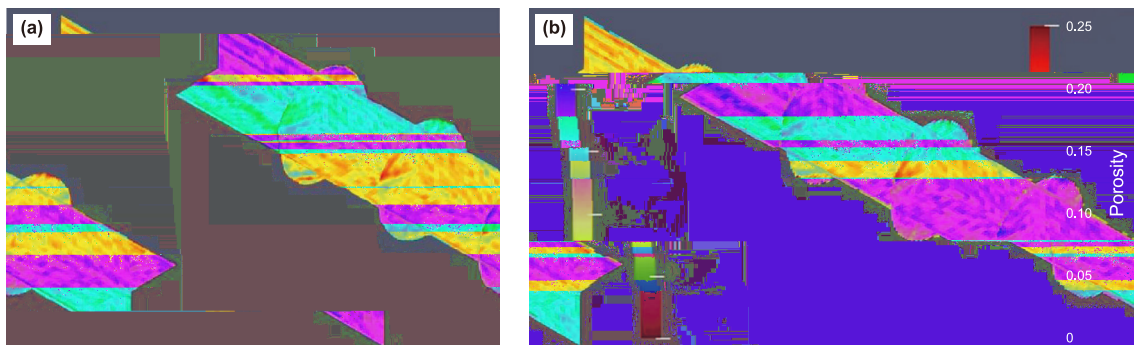


Fig. 11. Comparison of porosity distribution. (a) CT scanning; (b) Resampling.

well. One complete alternating cycle between SCW and CO₂ was set to 6 months. The injection well operates under constant-rate injection, with a daily injection volume of 18 m³ under reservoir conditions. The production well was constrained by a minimum bottom-hole pressure of 10 MPa and a daily fluid production rate of 18 m³.

3.3. Design of simulation schemes

The impacts of injection rate, water-to-gas ratio, and permeability contrast on SCWAG oil recovery and CO₂ storage efficiency were examined. In the single-factor analysis, only one factor was varied, while the other two were held constant. The simulation

schemes are presented in Table 4. Given the limited quantitative analysis in existing studies regarding the effects of each factor on recovery and CO₂ storage efficiency, and the absence of research on factor interactions, RSM was employed to quantify the influence of the three factors on SCWAG recovery and CO₂ storage efficiency, while accounting for interactions among the factors. Injection rate (A), water-to-gas ratio (B), and permeability contrast (C) were selected as input variables for the RSM central composite design. The three variables and their respective levels are presented in Table 5.

3.4. Simulation results analysis

3.4.1. Single-factor analysis

(1) Injection rate

Fig. 14 illustrates the variation in oil recovery and CO₂ storage efficiency with injection rate. As the injection rate increased, SCWAG recovery rose, while CO₂ storage efficiency decreased. Specifically, when the injection rate increased from 14 m³/day to 22 m³/day, recovery increased from 54.37% to 58.24%, whereas CO₂ storage efficiency decreased from 72.74% to 48.23%. The increase in gas injection rate results in a higher total injection volume, which enhanced oil displacement and, consequently, improved recovery. However, a high injection rate also increased viscous forces, which could destabilize the displacement front and increase the likelihood of gas breakthrough, leading to a significant decrease in CO₂ storage efficiency. Optimizing the injection rate is necessary to maximize both oil recovery and CO₂ storage efficiency. Additionally, the economic implications of high injection volumes should be considered when implementing this process in the field.

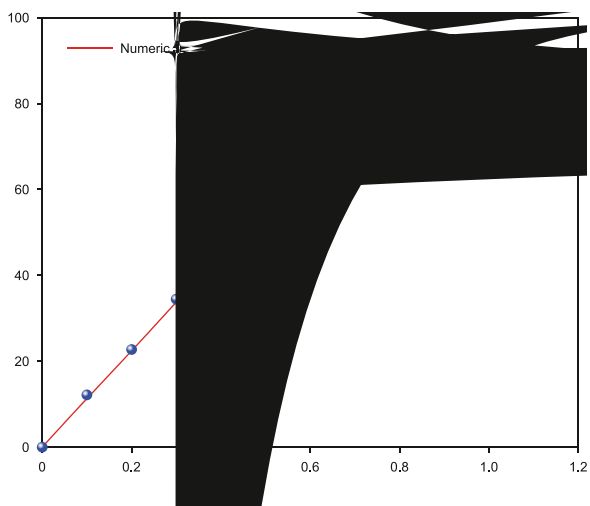


Fig. 12. Experimental and numerical simulation fitting results.

(2) Water-to-gas ratio



Fig. 13. Relative permeability curves fitted by CMOST. (a) Gas-liquid relative permeability; (b) Oil-water relative permeability.

The recovery and CO₂ storage efficiency results at different water-to-gas ratios are shown in Fig. 15. As the water-to-gas ratio increased, both recovery and CO₂ storage efficiency increased. When the water-to-gas ratio increased from 1:2 to 2:1, recovery increased from 54.47% to 57.09%, and CO₂ storage efficiency increased markedly from 48.93% to 72.12%. An increase in the water-to-gas ratio enhanced the control of water over the gas, which helped stabilize the gas displacement front. Additionally, it facilitated CO₂ dissolution and storage in water, thus increasing both oil recovery and CO₂ storage efficiency.

It is important to note that although this study showed that a water-to-gas ratio of 2:1 yielded better results than ratios of 1:1 and 1:2, a higher ratio is not always better. When the water-to-gas ratio is markedly low, the control of SCW over CO₂ is insufficient,

causing CO₂ to form a continuous phase and result in gas breakthrough, leading to low sweep efficiency (Lewis et al., 2008; Wang et al., 2020). For instance, in the simulations, defining gas breakthrough by a gas-oil ratio of 1500 m³/m³. Under this criterion, the 2:1 water-to-gas ratio delayed breakthrough by one year compared to the 1:2 ratio. Conversely, when the water-to-gas ratio is too high, the efficiency of oil displacement is reduced. Therefore, in practical reservoir development, the optimal water-to-gas ratio should be selected based on the specific characteristics of the reservoir.

(3) Permeability contrast

Fig. 16 illustrates the variations in oil recovery and CO₂ storage efficiency across different permeability contrasts. As the permeability contrast increases, recovery gradually decreases, whereas CO₂ storage efficiency initially increases before subsequently decreasing. A lower permeability contrast corresponds to weaker reservoir heterogeneity, which delays gas breakthrough and leads to higher oil recovery. However, the simulation model represented a positive rhythm reservoir. To ensure a controlled comparison, the overall permeability of the model was kept constant, while only the permeability contrast was varied. The smaller permeability contrast implied a relatively higher vertical permeability in the

Table 3

The properties of the reservoir model for the SCWAG simulation.

Parameter	Value
Average porosity, %	16.0
Average permeability, mD	15.0
Initial oil saturation, %	70.0
Grid block in x, y, z directions	50, 50, 6
Dimensions (x, y, z), m	5.64, 5.64, 3.0
Top depth, m	2200.0
Original formation pressure, MPa	25.0
Initial temperature, °C	72.0

Table 4

The simulation schemes of single-factor analysis.

Parameter	Scheme of simulation	Basic parameter value
Injection rate, m ³ /d	14, 16, 18, 20, 22	18
Water-to-gas ratio	1:2, 1:1.5, 1:1, 1.5:1, 2:1	1:1
Permeability contrast	2, 3.5, 5, 6.5, 8	5

Table 5

Input variables and levels for RSM.

Factor	Variable	Levels	
		Low	High
Injection rate, m ³ /d	A	14	22
Water-to-gas ratio	B	0.5	2
Permeability contrast	C	2	8

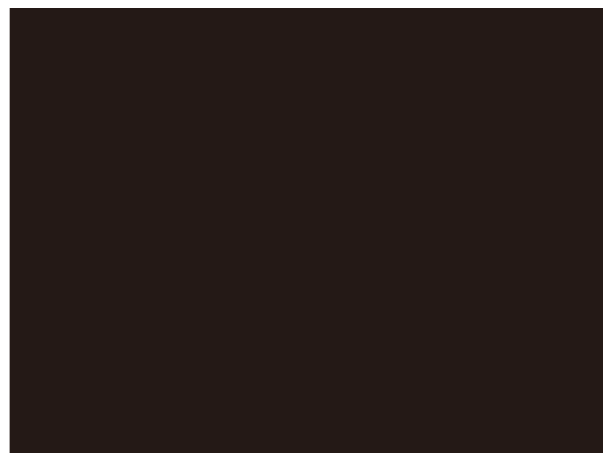


Fig. 14. Variation of recovery and CO₂ storage efficiency with injection rate.

ratio rose rapidly post-breakthrough. Consequently, while the oil recovery decreased from 60.94% to 53.84%, the CO₂ storage efficiency increased from 44.23% to 60.08%. However, upon a further increase in permeability contrast to 8.0, the intensified heterogeneity led to an earlier gas breakthrough, and as a result, both oil recovery and CO₂ storage efficiency declined to 51.69% and 57.83%, respectively. Therefore, the influence of permeability contrast on oil recovery and CO₂ storage efficiency is complex. To optimize oil recovery while achieving effective CO₂ storage, it is crucial to thoroughly consider the complex influences of permeability contrast on both oil recovery and CO₂ storage efficiency.

3.4.2. Sensitivity analysis

The P-values of the response surface analysis models for recovery (Y_1) and CO₂ storage efficiency (Y_2) were less than 0.001. Typically, a P-value below 0.05 indicates that the factor or model is statistically significant. Therefore, these models exhibited high statistical significance, excellent fit, and practical applicability. A scatter plot comparing predicted and actual values is shown in Fig. 17, where the close alignment further validates the reliability of the model. The F-value quantifies the contribution of each variable to the model, with a higher F-value indicating a greater influence of the corresponding factor (Afari et al., 2022). Generally, there is a correlation between the P-value and F-value, whereby a larger F-value corresponds to a smaller P-value.

Based on the F-values, the influencing factors were ranked, and significant factors were identified in conjunction with the P-values, as illustrated in Fig. 18. Factors A, B, and C each exerted a significant influence on both recovery (Y_1) and CO₂ storage efficiency (Y_2), underscoring the appropriateness of the selected fac

upper part of the reservoir; therefore, cases with low permeability contrast were more susceptible to gravity override. As the permeability contrast increased from 2.0 to 6.5, gas breakthrough was delayed compared to the highest-contrast case, but the gas-oil

storage efficiency requires focusing primarily on the injection rate and water-to-gas ratio.

Given the substantial influence of the interaction between the water-to-gas ratio and permeability contrast on both oil recovery and CO₂ storage efficiency, and their predominant effect among interacting factors, response surface plots for oil recovery and CO₂ storage efficiency as functions of factors B and C are presented in [Fig. 19](#). When permeability contrast remained constant, both oil recovery and CO₂ storage efficiency increased with an increasing water-to-gas ratio. Compared to low permeability contrast, the impact of the water-to-gas ratio on recovery o kpl w

performance have been thoroughly investigated. The findings provide new insights into the underlying mechanisms and offer crucial guidance for the design and implementation of SCWAG.

- (1) SCWAG flooding integrates the advantages of surfactants, CW, and CO₂. It not only suppresses gas channeling but also effectively mitigates the effect of water shielding. The zwitterionic surfactant and CW could mutually enhance each other, significantly improving wettability, reducing IFT, and promoting CO₂ mass transfer, thus facilitating EOR. The recovery of SCWAG is 76.99%, with recoveries for micropores, mesopores, and macropores of 56.35%, 76.85%, and 87.96%, respectively. The contribution of mesopores and macropores to recovery is substantial, while the improvement in micropores is particularly significant when compared to CO₂ flooding.
- (2) WAG flooding improves sweep efficiency, with CO₂ dissolving in trapped water, residual oil, and the injected water. The CO₂ storage efficiency was 55.60%, which was 8.93% higher than that of CO₂ flooding. Although CWAG helps alleviate the impact of water shielding and facilitates CO₂ mass transfer into oil, CW is less effective at continuously dissolving the injected CO₂, resulting in slightly lower CO₂ storage efficiency compared to WAG flooding. SCWAG, on the other hand, provides a larger pore space for CO₂ storage and further promoted CO₂ mass transfer, achieving a CO₂ storage efficiency of 57.22%.
- (3) A higher injection rate results in a larger injection volume, which is beneficial for improving recovery. However, a high injection rate is detrimental to maintaining the stability of the displacement front, leading to a decrease in CO₂ storage efficiency. As the water-to-gas ratio increases, SCW more effectively controls CO₂ flow, which is beneficial for improving both recovery and CO₂ storage efficiency. The impact of permeability contrast on SCWAG is complex. As permeability contrast increases, recovery declines, while the CO₂ storage efficiency initially increases and then decreases, as observed within the parameter range of this study.
- (4) Injection rate, water-to-gas ratio, and permeability contrast have a significant impact on both recovery and CO₂ storage efficiency, but their relative effects vary for each objective. Permeability contrast has the greatest impact on recovery, exceeding both the injection rate and water-to-gas ratio. In contrast, CO₂ storage efficiency is primarily influenced by the injection rate, which has a slightly greater impact than the water-to-gas ratio and a more pronounced impact than permeability contrast. Beyond these individual factors, the interaction between the water-to-gas ratio and permeability contrast should also be considered in SCWAG for low-permeability reservoirs.

Overall, SCWAG offers a promising approach to EOR and CO₂ storage through its ability to improve sweep efficiency and enhance oil displacement. Future research could explore the potential of integrating SCW with other agents, such as gels and foams, to improve its adaptability and performance in highly heterogeneous reservoirs. Furthermore, it would be worthwhile to investigate the development of novel surfactants that enhance CO₂ solubility in water and facilitate CO₂ mass transfer, potentially leading to further improvements in SCWAG performance.

CRediT authorship contribution statement

Xiao-Bing Han: Writing – original draft, Methodology, Investigation. **Hai-Yang Yu:** Writing – review & editing, Investigation,

Conceptualization. **Tong-Bing Wang:** Visualization, Software, Methodology. **Peng Song:** Validation, Resources, Conceptualization. **Jia-Bang Song:** Visualization, Software. **Lu Liu:** Visualization, Methodology, Formal analysis. **Hui-Ting Tang:** Validation, Methodology, Investigation. **Jun Lu:** Validation, Methodology, Formal analysis. **Yang Wang:** Writing – review & editing, Methodology.

Declaration of interests

The authors declare that they have no known competing financial interests or personal relationships that could have appeared to influence the work reported in this paper.

Acknowledgments

This work was financially supported by the National Science and Technology Major Project (2025ZD1406204) and the National Natural Science Foundation of China (52074317).

References

- Afari, S., Ling, K., Sennaoui, B., et al., 2022. Optimization of CO₂ huff-n-puff EOR in the Bakken Formation using numerical simulation and response surface methodology. *J. Petrol. Sci. Eng.* 215, 110552. <https://doi.org/10.1016/j.petrol.2022.110552>.
- Afzali, S., Rezaei, N., Zendejboudi, S., 2018. A comprehensive review on Enhanced oil recovery by water alternating gas (WAG) injection. *Fuel* 227, 218–246. <https://doi.org/10.1016/j.fuel.2018.04.015>.
- Akin, S., Kovscek, A.R., 2003. Computed tomography in petroleum engineering research. *Geological Society* 215 (1), 23–38. <https://doi.org/10.1144/GSL.SP.2003.215.01.03>.
- Alabdulbari, O.A.A., Alabid, F.S.R., Hosseini, S., 2022. Effects of formation brine, [C₁₂mim][Cl] concentration, temperature and pressure on the swelling factor and IFT of the carbonated water/heavy crude oil system. *Braz. J. Chem. Eng.* 39 (1), 289–300. <https://doi.org/10.1007/s43153-021-00210-6>.
- Bai, M.X., Zhang, Z.C., Yang, E.L., et al., 2025. Experimental study of microscopic oil production and CO₂ storage in low-permeable reservoirs. *Pet. U. O. O. cP. k. DUE. p¹R*

- Ji, M., Kwon, S., Choi, S., et al., 2023. Numerical investigation of CO₂-carbonated water-alternating-gas on enhanced oil recovery and geological carbon storage. *J. CO₂ Util.* 74, 102544. <https://doi.org/10.1016/j.jcou.2023.102544>.
- Kumar, S., Mandal, A., 2017. A comprehensive review on chemically enhanced water alternating gas/CO₂ (CEWAG) injection for enhanced oil recovery. *J. Petrol. Sci. Eng.* 157, 696–715. <https://doi.org/10.1016/j.petrol.2017.07.066>.
- Kumar, N., Pal, N., Mandal, A., 2021. Nanoemulsion flooding for enhanced oil recovery: theoretical concepts, numerical simulation and history match. *J. Petrol. Sci. Eng.* 202, 108579. <https://doi.org/10.1016/j.petrol.2021.108579>.
- Lee, J.H., Jeong, M.S., Lee, K.S., 2017. Geochemical modelling of carbonated low salinity water injection CLSWI to improve wettability modification and oil swelling in carbonate reservoir. In: *SPE Latin America and Caribbean Mature Fields Symposium*. <https://doi.org/10.2118/184915-MS>.
- Lee, Y., Kim, S., Wang, J., et al., 2020. Relationship between oil production and CO₂ storage during low-salinity carbonate water injection in acid carbonate reservoirs. *J. Ind. Eng. Chem.* 88, 215–223. <https://doi.org/10.1016/j.jiec.2020.04.016>.
- Lewis, E., Dao, E.K., Mohanty, K.K., 2008. Sweep efficiency of miscible floods in a high-pressure quarter-five-spot model. *SPE J.* 13 (4), 432–439. <https://doi.org/10.2118/102764-PA>.
- Li, Y.K., Nghiem, L.X., 1986. Phase equilibria of oil, gas and water/brine mixtures from a cubic equation of state and henry's law. *Can. J. Chem. Eng.* 64 (3), 486–496. <https://doi.org/10.1002/cjce.5450640319>.
- Lin, Q.Y., Zhang, X., Wang, T., et al., 2022. Technical perspective of carbon capture, utilization, and storage. *Engineering* 14, 27–32. <https://doi.org/10.1016/j.eng.2021.12.013>.
- Liu, Y.L., Rui, Z.H., 2022. A storage-driven CO₂ EOR for a net-zero emission target. *Engineering* 18, 79–87. <https://doi.org/10.1016/j.eng.2022.02.010>.
- Liu, J.R., Zhang, D.F., Liu, S.Y., et al., 2025. Multiscale investigation into EOR mechanisms and influencing factors for CO₂-WAG injection in heterogeneous sandy conglomerate reservoirs using NMR technology. *Pet. Sci.* 22 (7), 2977–2991. <https://doi.org/10.1016/j.petsci.2025.04.004>.
- Luo, X.J., Wei, B., Gao, K., et al., 2023. Gas channeling control with an in-situ smart surfactant gel during water-alternating-CO₂ enhanced oil recovery. *Pet. Sci.* 20 (5), 2835–2851. <https://doi.org/10.1016/j.petsci.2023.03.003>.
- Lyu, X.C., Voskov, D., Tang, J.Y., et al., 2021. Simulation of foam enhanced-oil-recovery processes using operator-based linearization approach. *SPE J.* 26 (4), 2287–2304. <https://doi.org/10.2118/205399-PA>.
- Majidaie, S., Khanifar, A., Onur, M., et al., 2012. A simulation study of chemically enhanced water alternating gas CWAG injection. In: *SPE EOR Conference at Oil and Gas West Asia*. <https://doi.org/10.2118/154152-MS>.
- Nghiem, L.X., Aziz, K., Li, Y.K., 1983. A robust iterative method for flash calculations using the soave-redlich-kwong or the Peng-Robinson equation of state. *Soc. Petrol. Eng. J.* 23 (3), 521–530. <https://doi.org/10.2118/8285-PA>.
- Nowrouzi, I., Manshad, A.K., Mohammadi, A.H., 2019. Effects of dissolved carbon dioxide and ions in water on the dynamic interfacial tension of water and oil in the process of carbonated smart water injection into oil reservoirs. *Fuel* 243, 569–578. <https://doi.org/10.1016/j.fuel.2019.01.069>.
- Nowrouzi, I., Mohammadi, A.H., Manshad, A.K., 2020. Utilization of methanol and acetone as mutual solvents to reduce interfacial tension (IFT) in enhanced oil recovery process by carbonated smart water injection. *J. Mol. Liq.* 304, 112733. <https://doi.org/10.1016/j.molliq.2020.112733>.
- Ren, B., Duncan, I.J., 2021. Maximizing oil production from water alternating gas (CO₂) injection into residual oil zones: the impact of oil saturation and heterogeneity. *Energy* 222, 119915. <https://doi.org/10.1016/j.energy.2021.119915>.
- Riazi, M., Golkari, A., 2016. The influence of spreading coefficient on carbonated water alternating gas injection in a heavy crude oil. *Fuel* 178, 1–9. <https://doi.org/10.1016/j.fuel.2016.03.021>.
- Sarkar, R., Das, A., Rakshit, A., et al., 202